International Journal of Mathematical, Engineering and Management Sciences
Vol. 11, No. 1, 242-268, 2026
https://doi.org/10.33889/IJMEMS.2026.11.1.011

Enhanced Thermal Efficiency Using Hybrid Nanofluids in MHD Boundary Layer Flow: Buoyancy and Entropy Perspective

Ch Santosh
Department of Mathematics,
Siksha 'O' Anusandhan University, Bhubaneswar, 751030, Odisha, India.
Corresponding author: chsantosh206@gmail.com

S. K. Parida
Department of Mathematics,
Siksha 'O' Anusandhan University, Bhubaneswar, 751030, Odisha, India.
E-mail: sampadaparida@soa.ac.in

(Received on June 29, 2025; Revised on September 7, 2025 & November 11, 2025; Accepted on November 13, 2025)

Abstract
The growing relevance of hybrid nanofluids (HNFs) in advanced thermal management systems has driven extensive research in recent years. Nevertheless, the cumulative effects of thermal and solutal buoyancy, MHD, viscous dissipation, and Newtonian heating/cooling on HNF transport remains unaddressed. Motivated by their significance in solar energy systems, electronic cooling, and chemical reactors, this study presents a comprehensive numerical investigation of magnetohydrodynamic (MHD) hybrid nanofluid flow over a porous stretching sheet, incorporating the combined effects of thermal and solutal buoyancy forces, Newtonian heating/cooling, viscous dissipation, and heat generation/absorption. The hybrid nanofluid (Cu/Al_2O_3-water) is modelled using the Tiwari–Das approach. The governing PDEs are transformed into ODEs through similarity transformations and solved using a finite-difference-based Runge–Kutta–Fehlberg method in MATLAB. The analysis reveals that both thermal and solutal buoyancy significantly enhance fluid temperature while reducing nanoparticle concentration through stronger convective transport. The skin-friction coefficient enhances with the copper nanoparticle volume fraction but decreases with solutal buoyancy. The hybrid nanofluid demonstrates superior heat-transfer performance, with up to a 16% higher Nusselt number compared to single nanofluids, making it ideal for thermal regulation in microchannel heat sinks and renewable energy systems. Validation against prior literature confirms the model's accuracy.

Keywords- Hybrid nanofluid, Newtonian heating/cooling, Buoyancy effect, Joule heating, Viscous dissipation, Stretching sheet.

1. Introduction

The study of extrusion techniques in engineering and technology, the motion of biological fluids, glass fibre manufacturing, and lubrication processes such as the forcing out of plastic has gained significant recognition in recent decades. Much of this attention has been directed towards investigating flow behaviour over stretching surfaces. The pioneering work of Siddappa and Abel (1985) examined boundary-layer flow over a stretching sheet, while Mahapatra and Gupta (2002) studied the behaviour of incompressible viscous fluids over a deformable surface. Subsequent studies, including those by Vajravelu and Rollins (1992) and Wang and Mujumdar (2007), highlighted the thermal behaviour and flow properties of fluids across stretching surfaces under various physical effects. These studies collectively established stretching-sheet flows as a central model for analysing boundary-layer transport.

Building on this foundation, researchers broadened their studies to nanofluids, further aiming to enhance mass and heat transfer in stretching sheet configurations. Keblinski et al. (2002) demonstrated that classical macroscopic theories fail to explain the experimentally observed thermal conductivity enhancement and proposed new mechanisms such as Brownian motion and liquid layering. When Oztop and Abu-Nada (2008) studied nanofluids in natural convection enclosures, they discover a significant

increase in heat transmission. Khan and Pop (2010) investigated boundary layer nanofluid flow past a stretching surface and reported significant enhancement in thermal transport compared to pure fluids. More recently, Turkyilmazoglu (2024b) revealed new time-dependent solutions for unsteady stretching/shrinking sheet flows, while Turkyilmazoglu (2024a) investigated nonlinear similarity flows triggered by stretching/moving sheets with applications in electrospinning and atomization. These works show the relevance of stretching-sheet models in modern industrial processes.

Although nanofluids provided notable advancements, researchers later developed hybrid nanofluids to achieve even higher thermal efficiency. Suresh et al. (2012) experimentally carried-out studies on the convective heat transport of (Cu/Al_2O_3 water) hybrid-nanofluid in a evenly heated circular-tube and discovered higher heat transfer rates with only a slight increase in skin friction compared to single nanofluids. Devi and Devi (2017) found a 11% enhancement in Nusselt number for hybrid nanofluids over nanofluids and 17.3% over water. Aly et al. (2023) investigated hybrid-nanofluid flow across a sheet, incorporating viscous-dissipation and partial slip, revealing significant improvement in heat-transfer. Researchers (Varatharaj et al., 2024; Khan et al., 2025) investigated hybrid- nanofluid flow and discovered that they are more efficient than nanofluids and pure water, making them suitable for advanced cooling applications.

With the emergence of hybrid nanofluids, entropy generation and slip effects became crucial factors for modeling nanoscale and microscale transport. Ibrahim and Shankar (2013) examined the slip flow of nanofluids across permeable stretching sheets, and noticed reduction in heat transport as well as velocity. Under slip conditions, Varatharaj et al. (2025) showed that ternary hybrid nanofluids further enhance heat transfer over stretching sheet, verifying the increasing efficiency of multi-component nanoparticle systems. Researchers (Naqvi et al., 2024, Sakkaravarthi and Reddy, 2024, Hayat et al., 2024) highlighted the outcomes of boundary conditions and slip effects on entropy generation in a range of nanofluids. Considering convective and thermal slip conditions, Kandukoori et al. (2025) studied HNF (*MgO-ZnO/*water) transport over exponentially stretching sheet with viscous dissipation, focusing entropy generation. Abrar et al. (2025) numerically studied the entropy optimization of in tangent hyperbolic fluid flow over stretching sheet, demonstrating that entropy generation increases with Brinkman number, and Darcy dissipation with applications in water soil infiltration and oil recovery, while Aziz et al. (2020) considering velocity slip conditions, analysed the entropy, heat transfer of electrically conducting hybrid nanofluid over stretching horizontal surface. Arif et al. (2023) illustrated the physical-perception of entropy generation in a curved-surface with cross diffusion and transpiration. In the findings, it is culminated that in case of blood-based hybrid-nanofluid the heat transfer rate is 19.16% whereas there is an enhancement of 16.42% in case of menthol-based hybrid-nanofluid. Using the Eyring-Powell model, Ogunseye et al. (2020) looked into entropy production in the viscous hybrid-nanofluid flow, revealing hybrid-nanofluid have enhanced thermal characteristics in comparison to regular fluid. Acharya et al. (2022) explored entropy generation on flow of unsteady hybrid nanofluid over a rotating disc with slip. As slip effects gained prominence, attention also shifted to magnetic fields, which play a decisive role in modifying nanofluid and hybrid nanofluid transport.

The application of MHD in nanofluids is vital for controlling thermal and electromagnetic flow. Abbas et al. (2024) analyzed second-grade nanofluid flow over an inclined surface under the combined effects of MHD and porosity. Santosh and Parida (2023) investigated MHD nanofluid flow with heat generation over nonlinearly stretching sheets, revealing mechanisms for controlling thermal profiles. Turkyilmazoglu and Alotaibi (2025) examined asymptotic MHD viscous flow through porous-walled pipes. Sobale et al. (2025) focused on flow of MHD ternary hybrid nanofluid under the effects of viscous dissipation, radiation over stretched sheet and findings shows that ternary HNF shows enhanced heat transfer. Uygun

and Turkyilmazoglu (2025) investigated MHD Bingham fluid flow over rotating disks regulated by electric fields. Khalatbari et al. (2025) thoroughly evaluates the most recent studies on hybrid nanofluids, providing novel insights into their design methodologies and thermophysical characteristics. To further improve such models, buoyancy effects both solutal and thermal have been incorporated, as they are fundamental convection drivers in nanofluid systems.

Thermal buoyancy refers to the buoyant force generated within a fluid due to temperature variations. Solutal buoyancy, also known as compositional or concentration buoyancy, is the buoyant effect generated by solute concentration changes in a fluid. Abdelhafez et al. (2024) studied EMHD flow with thermal buoyancy effects over a stretched-sheet in porous media, exhibiting strong temperature enhancement. Incorporating buoyancy effects, Rafique et al. (2025) investigated the stagnation point flow of an Al_2O_3–Cu/H_2O fluid over an inclined-cylinder, revealing buoyancy-driven dual solutions. Waini et al. (2021) enlightened hybrid-nanofluid flow on an exponentially shrinking/stretching sheet and reported bifurcation behaviour due to buoyancy reversal. Tanuja et al. (2024) investigated the flow behaviour of a HNF composed of tin oxide and silica nanoparticles dispersed in engine oil, flowing through porous-media adjacent to a semi-infinite flat plate. Following Darcy–Brinkman model, Khan et al. (2021) inquire into the results of buoyant force on hybrid-nanofluid stream in the saturated porous media over a plate placed vertically. The results are distinct for Positive buoyant flow ($\lambda c < 0$), but has dual or many outcomes occur for buoyancy-opposing flow ($\lambda c < 0$). Two kinds of HNFs were considered by Rana et al. (2023), who compared and evaluated the thermal-transport performance of these two sets of HNFs in the presence of buoyant-force. Owing to their practical relevance, Researchers (Farooq et al., 2024; Mahmood et al., 2025) enlightens the effects of buoyant force and entropy generation of HNF flows across various media. Abdou and Al-Wtheeh (2025) examined flow of nanofluid (Cu–water) along a vertical surface in non-Darcian porous-media, accounting for Joule heating, viscous dissipation, suction/injection, buoyancy effects on mass and heat transfer.

1.1 Research Gap and Present Study

Although many studies have examined hybrid nanofluid flow over stretching sheets, the combined effects of thermal and solutal buoyancy, Newtonian heating/cooling, and viscous dissipation in HNFs remain insufficiently explored. Most existing work overlooks these interactions, limiting understanding of coupled heat and mass transfer under realistic boundary conditions. This study addresses this gap by analyzing the buoyancy-driven HNF flow with Newtonian thermal effects over a stretching surface by the expanding the findings of Joyce et al. (2023). The interplay of mass & heat transfer along with buoyancy effects is crucial in several practical usages to enhance the efficiency and effectiveness of various thermal and chemical processes.

The parameters incorporated in this study is given in the **Table 1** and are chosen because they directly affect momentum, solutal and thermal transport in boundary layer flows and are essential to industrial and engineering processes.

The novel findings of the current study are listed below.:

- In HNF flow, incorporation of solutal and thermal buoyancy in momentum equation, has rarely been overlooked together, especially for (Cu/Al_2O_3 water) mixture.
- Inclusion of heat source/sink and viscous dissipation in the energy equation, create a more realistic model of energy transport in engineering applications.
- Convective boundary-conditions are used.
- The shooting technique in conjunction with Runge-Kutta-Fehlberg's scheme to solve the mathematical model.

- Comparison of single nanoparticle nanofluids with the HNF, emphasising performance benefits.

Table 1. Applications of parameters and its physical significance.

Parameter	Meaning	Applications
Joule heating	Heat generated due to electrical resistance in magnetic fields	nuclear fusion systems, MHD devices, electronic cooling
Buoyancy Force (Thermal and Solutal)	Generates natural/mixed convection due to temperature and concentration variations	electronic devices, Cooling of solar-collectors, nuclear reactors
Heat source/sink	Internal energy generation/absorption	Chemical reactors, combustion chambers, solar absorbers
Viscous Dissipation	Conversion of Kinetic energy to internal energy	electronic cooling, lubrications MHD devices
Velocity Slip	Non zero velocity relative to solid surface at the boundary	biomedical flow, Micro/nano-scale devices
Newtonian heating/cooling	heat exchange through convection	heat exchangers, solar energy collectors

2. Mathematical Description

Consider a 2D, steady and incompressible flow of hybrid-nanofluid composed of two types of NPs, Copper (Cu) and Aluminium Oxide (Al_2O_3), over a porous stretching sheet as illustrated in **Figure 1**. These two NPs have varied range of industrial and engineering applications as mentioned in literature. The associated thermophysical-properties are shown in **Table 2** and the effective thermophysical properties for hybrid-nanofluid are shown in **Table 3**.

The energy equation governs the thermal field. Beyond convection and conduction, Heat transfer is affected by many irreversible mechanisms like viscous dissipation, heat source/sink, joule heating. Therefore, it is physically and naturally acceptable to incorporate more terms in energy equation. In the present model, it is empowered by heat sink/source and viscous dissipation terms. With the addition of these terms, the thermal analysis becomes more relevant and practical in engineering applications such as nuclear/solar thermal systems, polymer extrusion and electromagnetic cooling devices.

The coordinate system is specified such that the x-axis is taken along the stretching sheet and the y-axis is normal to it. The sheet is stretched at a steady pace $u_w(x) = ax$ with $a > 0$, where a is stretching rate. Here T_∞ : ambient temperature, C_∞ : ambient-concentration.

The following assumptions are made:

- The hybrid-nanofluid is assumed to be incompressible and Newtonian.
- The state of fluid and NPs are in thermal-equilibrium.
- Since the induced magnetic-field is minimal, it is neglected.

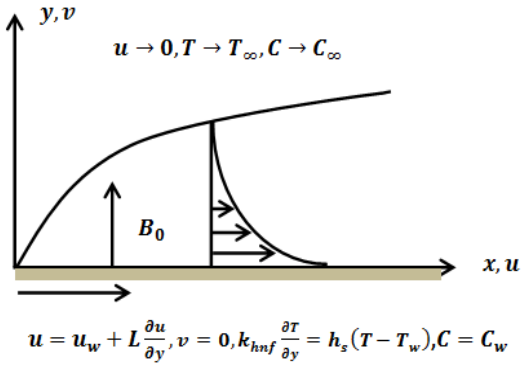

Figure 1. Problem's physical model.

Under the above assumptions, the governing equations for conservative momentum, energy, & concentration in a steady 2D flow of a hybrid nanofluid are:

$$\frac{\partial u}{\partial x}+\frac{\partial v}{\partial y}=0 \tag{1}$$

$$u\frac{\partial u}{\partial x}+v\frac{\partial u}{\partial y}=\frac{1}{\rho_{hnf}}\left[\mu_{hnf}\left(\frac{\partial^2 u}{\partial y^2}-\frac{u}{k^*}\right)-\sigma_{hnf}B_0{}^2u+g\left(\rho\beta\right)_{hnf}\left(T-T_\infty\right)+g\left(\rho\beta\right)_{hnf}\left(C-C_\infty\right)\right] \tag{2}$$

$$u\frac{\partial T}{\partial x}+v\frac{\partial T}{\partial y}=\frac{1}{\left(\rho C_p\right)_{hnf}}\left[k_{hnf}\frac{\partial^2 T}{\partial y^2}+\sigma_{hnf}B_0{}^2u^2+\mu_{hnf}\left(\frac{\partial u}{\partial y}\right)^2+q\left(T-T_\infty\right)\right] \tag{3}$$

$$u\frac{\partial C}{\partial x}+v\frac{\partial C}{\partial y}=D_M\left(\frac{\partial^2 C}{\partial y^2}\right)\text{-}k_r\left(C-C_\infty\right) \tag{4}$$

The associated boundary-conditions are

$$\left.\begin{array}{l} u=u_w+u_{slip}=u_w+L\left(\dfrac{\partial u}{\partial y}\right),\ k_{hnf}\left(\dfrac{\partial T}{\partial y}\right)=h_s\left(T-T_w\right),v=v_w=0,\ C=C_w\ \ at\ y=0 \\ T\to T_\infty,u\to 0,C\to C_\infty\ \ \ as\ y\to\infty \end{array}\right\} \tag{5}$$

Here C, T denotes concentration and temperature of the hybrid-nanofluid, while v, u are velocities along y-axis and x-axis respectively. Furthermore, D_M, k_r, B_0, k^* represents mass diffusivity, rate of chemical-reaction, magnetic-field strength, and permeability of porous-media.

The boundary conditions in Equation (5) are explained as follows:

At $\eta = 0$, velocity slip condition (partial slip effects) is incorporated where velocity of fluid is inconsistent with sheet velocity, but is proportional to the rate of change of velocity near the wall, play a key role in nano and micro-scale flows. Thermal boundary condition is of convective type, where the temperature at the wall is determined by heat transfer with the ambient medium. The no-penetration condition assures with no suction/injection across its surface. The solutal concentration at the surface is specified to control how mass is moved at the wall.

At $\eta\to\infty$, the concentration and temperature tend to their respective ambient conditions, whereas velocity approaches the free-stream value.

Table 2. Thermo-physical properties of nano-particles & water (El-Dawy and El-Amin, 2021; Krishna et al., 2021).

Properties	**σ (s / m)**	**k (W/mK)**	**Cp(J/kgK)**	**ρ (kg/m^3)**
Al_2O_3	3.69 x 10^7	40	765	3970
Cu	5.96 x 10^7	400	385	8933
water	5.5 x 10-6	0.613	4180	997.1

Copper and Aluminium oxide nanoparticles are incorporated in this study due to the complementary thermophysical properties. Al_2O_3 nanoparticles (NPs) enhance the heat absorption and suspension stability by providing high specific heat, superior chemical stability and lower cost. In contrast, Copper nanoparticles show high thermal conductivity (around $400W\ /\ mK$) which enhances the suspension capacity to transfer heat. The combination of Al_2O_3 and Cu nanoparticles dispersed in water guarantees

both enhanced thermal conductivity and stable dispersion, making the hybrid nanofluid particularly suitable for applications such as electronic cooling, solar collectors, and advanced heat exchangers and microchannel heat sinks.

Table 3. Thermo-physical properties of HNF following (El-Dawy and El-Amin, 2021; Krishna et al., 2021).

Properties	**Hybrid-Nanofluid**
Heat capacity	$(\rho C_p)_{hnf} = \phi_2(\rho C_p)_2 + (1-\phi_2)[(1-\phi_1)(\rho C_p)_f + \phi_1(\rho C_p)_1]$
Electrical conductivity	$\frac{\sigma_{hnf}}{\sigma_{nf}} = 1 + \frac{3\{(\sigma_2/\sigma_f)-1\}\phi_2}{\frac{\sigma_2}{\sigma_f}+2-\{(\sigma_2/\sigma_f)-1\}\phi_2}$ where $\frac{\sigma_{nf}}{\sigma_f} = 1 + \frac{3\{(\sigma_1/\sigma_f)-1\}\phi_1}{\frac{\sigma_1}{\sigma_f}+2-\{(\sigma_1/\sigma_f)-1\}\phi_1}$
Density	$\rho_{hnf} = (1-\phi_2)[(1-\phi_1)\rho_f + \phi_1\rho_1] + \phi_2\rho_2$
Dynamic- viscosity	$\mu_{hnf} = \frac{\mu_f}{(1-\phi_1)^{2.5}(1-\phi_2)^{2.5}}$
Thermal conductivity	$\frac{k_{hnf}}{k_{nf}} = \frac{k_2 + 2k_{nf} - 2\phi_2(k_{nf}-k_2)}{k_2 + 2k_{nf} + \phi_2(k_{nf}-k_2)}$ where $\frac{k_{nf}}{k_f} = \frac{k_1 + 2k_f - 2\phi_1(k_f-k_1)}{k_1 + 2k_f + \phi_1(k_f-k_1)}$

Following (Devi and Devi, 2017; Krishna et al., 2021) for a numerical solution of Equations (1) - (5) by the appropriate similarity variables as follows:

$$\left.\begin{aligned} &\psi(\eta) = x\sqrt{av_f}\,f(\eta), u = \frac{\partial\psi}{\partial y}, v = -\frac{\partial\psi}{\partial x}, \eta = \sqrt{a/v_f}\,y, \\ &v = -\sqrt{av_f}\,f(\eta)y, u = axf'(\eta), \theta(\eta) = \frac{T-T_\infty}{T_w-T_\infty}, \varphi(\eta) = \frac{C-C_\infty}{C_w-C_\infty} \end{aligned}\right\} \tag{6}$$

Using the Equation (6), the Equations (1) – (5) becomes

$$f''' - Kpf' + \frac{\mu_f}{\mu_{hnf}}\left[\frac{\rho_{hnf}}{\rho_f}\left(ff'' - f'^2\right) - \frac{\sigma_{hnf}}{\sigma_f}Mf' + \frac{\rho_{hnf}}{\rho_f}\left[Gr\,\theta + Gc\,\phi\right]\right] = 0 \tag{7}$$

$$\frac{\left(\rho C_p\right)_f}{\left(\rho C_p\right)_{hnf}}\left[\frac{k_{hnf}}{k_f}\frac{1}{Pr}\theta'' + \frac{\sigma_{hnf}}{\sigma_f}M\,Ec\,f'^2 + \frac{\mu_{hnf}}{\mu_f}Ec\,f''^2\right] + f\theta' + Q\theta = 0 \tag{8}$$

$$\phi'' + Sc\left(f\phi - K_r\phi\right) = 0 \tag{9}$$

The BCs are:

$$\left.\begin{aligned} &f'(0) = 1 + \lambda f''(0), \theta'(0) = -\frac{k_f}{k_{hnf}}Bi\left\{1-\theta(0)\right\}, f(0) = 0, \phi(0) = 1\,at\,\eta = 0 \\ &\theta(\infty) = 0, f'(\infty) = 0, \phi(\infty) = 0\,\text{as}\,\eta \to \infty \end{aligned}\right\} \tag{10}$$

where, $K_r = \frac{k_r}{a}, Sc = \frac{\nu_f}{D_M}, Pr = \frac{\nu_f}{\alpha_f}, M = \frac{\sigma B_0^{\,2}}{a\rho_f}, Ec = \frac{a^2x^2}{\left(T_w - T_\infty\right)\left(C_p\right)_f}, Bi = \frac{h_s}{k_f}, Kp = \frac{\nu_f}{ak^*},$

$\lambda = L\sqrt{\frac{a}{\nu_f}}, Q = \frac{q}{\left(\rho C_p\right)_{hnf} a}, Gr = \frac{g\beta_{hnf}}{au_w}\left(T_w - T_\infty\right), Gc = \frac{g\beta_{hnf}}{au_w}\left(C_w - C_\infty\right)$ are chemical reaction parameter, Schimdt number, Prandtl number, magnetic parameter, Eckert number, Biot number, porosity parameter, slip parameter, heat source/sink parameter, thermal and solutal Grashof numbers respectively.

The nonlinear Equations (7) - (9) with the boundary conditions (10) comprises a well posed boundary value problem. The governing equations satisfy the Lipchitz-Continuity in the permissible domain and are smooth. So, by Picard-Lindelof theorem, the transformed initial value problem which is solved by Shooting technique possesses a unique solution. Also, only one velocity, temperature, and concentration profile can satisfy both free-stream behaviour and wall conditions. More than one solution indicates different flow states in the same conditions, which is impractical for this type of laminar boundary layer problems.

The skin friction coefficient, Nusselt and Sherwood numbers are the physical quantities of engineering interest and are defined as

$$\left.\begin{aligned} Cf_x &= \frac{\tau_w}{\rho u_w^2} \Rightarrow \mathrm{Re}_x^{1/2}\, Cf_x = \frac{\mu_{hnf}}{\mu_f} f''(0), \\ Nu_x &= \frac{xq_w}{k\left(T_w - T_\infty\right)} \Rightarrow \mathrm{Re}_x^{-1/2}\, Nu_x = -\frac{k_{hnf}}{k_f}\theta'(0) \\ Sh_x &= \frac{xq_m}{D_M\left(C_w - C_\infty\right)} \Rightarrow \mathrm{Re}_x^{-1/2}\, Sh_x = -\phi'(0) \end{aligned}\right\} \quad (11)$$

where, $\tau_w = \mu_{hnf}\left(\frac{\partial u}{\partial y}\right)_{y=0}, q_w = -k_{hnf}\left(\frac{\partial T}{\partial y}\right)_{y=0}, q_w = -D_M\left(\frac{\partial C}{\partial y}\right)_{y=0}$ and $\mathrm{Re}_x = \frac{u_w x}{\nu}$ are surface shear stress, heat flux, mass flux and local Reynolds number respectively.

3. Entropy Generation

In MHD viscous flow, entropy generation arises due to several irreversible effects such as:

- Heat conduction through finite temperature gradients,
- Viscous dissipation from fluid friction,
- Ohmic (Joule) heating due to interaction of the magnetic field with the conducting fluid.

For this study, the Volumetric entropy generation rate is given as

$$E_G = \underbrace{\frac{k_{hnf}}{T_\infty^2}\left(\frac{\partial T}{\partial y}\right)^2}_{Thermal\ irreversibility} + \underbrace{\frac{\left(\sigma_{hnf} B_0^2\right)}{T_\infty} u^2}_{Joule\ dissipation\ irreversibility} + \underbrace{\frac{\mu_{hnf}}{T_\infty}\left(\frac{\partial u}{\partial y}\right)^2}_{Nanofluid\ friction\ irreversibility} + \underbrace{\frac{\mu_{hnf}}{T_\infty k^*} u^2}_{Porosity\ irreversibility} + \underbrace{\frac{RD_M}{T_\infty}\left(\frac{\partial C}{\partial y}\frac{\partial T}{\partial y}\right) + \frac{RD_M}{C_\infty}\left(\frac{\partial C}{\partial y}\right)^2}_{Nanoparticle\ mass\ transfer\ irreversibility} \tag{12}$$

The entropy generation characteristic is

$$E_0 = \frac{a\left(T_w - T_\infty\right)k_f}{T_\infty \upsilon_f},$$

and

$N_G = \frac{E_G}{E_0} = \frac{k_{hnf}}{k_f} A\theta'^2 + \frac{\sigma_{hnf}}{\sigma_f} M\, Br\, f'^2 + B\left[\phi'\theta' + \frac{A'}{A}\phi'^2\right] + \frac{\mu_{hnf}}{\mu_f} Br\left[\frac{f'}{E} + f''^2\right]$ is entropy-generation number.

where, $Br = \frac{\mu_f a^2 x^2}{k_f\left(T_w - T_\infty\right)}, B = \frac{RD_M}{k_f}\left(C_w - C_\infty\right), A = \frac{T_w - T_\infty}{T_\infty}, A' = \frac{C_w - C_\infty}{C_\infty}$.

Here, A and A' are temperature and concentration difference parameter, Br is Brinkman number, and B is Diffusion Parameter.

The Bejan number represents the fraction of mass and heat transport to overall entropy.

$$Be = \frac{\frac{k_{hnf}}{k_f} A\theta'^2 + B\left[\phi'\theta' + \frac{A'}{A}\phi'^2\right]}{\frac{k_{hnf}}{k_f} A\theta'^2 + \frac{\sigma_{hnf}}{\sigma_f} M\, Br\, f'^2 + B\left[\phi'\theta' + \frac{A'}{A}\phi'^2\right] + \frac{\mu_{hnf}}{\mu_f} Br\left[\frac{f'}{E} + f''^2\right]} \tag{13}$$

Therefore, it is evident from (13) that Be is in the range between 0 and 1. It is implied that heat transmission predominates over irreversibility when $Be >> 0.5$. The irreversibility is brought on by porosity, viscous dissipation & Joule-heating for $Be << 0.5$. This suggests that irreversibility resulting from heat-transfer, porosity, Joule heating, & viscous-dissipation are similar when $Be = 0.5$.

The analysis on Entropy generation is incorporated to analyse the thermodynamic efficiency of the hybrid nanofluid system. It gives a measure of irreversibility in mass and heat transfer processes, which is crucial in cooling and energy applications. The balance between enhanced heat transfer and entropy minimization is central to the present investigation. In the present model, higher entropy generation reflects stronger irreversibilities due to mechanisms such as buoyancy forces, Joule heating, and viscous dissipation, which reduce the thermal efficiency of the system. Conversely, lower entropy generation indicates minimal irreversibility, resulting in more efficient mass and heat transfer. Thus, evaluating entropy generation offers insights into the energy efficiency and optimization of hybrid nanofluid-based engineering systems.

4. Numerical Solution

The non-linear coupled ODEs (7) - (9) with BCs (10) are numerically resolved using Runge-Kutta Fehlberg's approach with the Shooting technique. This method (also known as the Fehlberg-method) is a numerical algorithm used to solve ODEs. It is a 4th order method equipped with a 5th order error estimator. The overall numerical procedure adopted for the present computation is illustrated in **Figure 2**.

The algorithm is as follows:

Step 1: Conversion of BVP to IVP:

Firstly, this approach converts the boundary value problem (BVP) into a system of first-order IVP, and are:

$$\left.\begin{aligned} f' &= p \\ p' &= q \\ q' &= Kp(p) - \frac{\mu_f}{\mu_{hnf}}\left[\frac{\rho_{hnf}}{\rho_f}\left(fq - p^2\right) - \frac{\sigma_{hnf}}{\sigma_f}Mp + \frac{\rho_{hnf}}{\rho_f}\left[Gr\,\theta + Gc\,\phi\right]\right] \\ \theta' &= s \\ s' &= -\frac{1}{a_1}\left\{\left[\frac{\sigma_{hnf}}{\sigma_f}M\,Ec\,p^2 + \frac{\mu_{hnf}}{\mu_f}Ec\,q^2\right] + \frac{\left(\rho C_p\right)_f}{\left(\rho C_p\right)_{hnf}}\left[fs + \lambda\theta\right]\right\} \\ \phi' &= w \\ w' &= Sc\left[K_r\phi - fw\right] \end{aligned}\right\} \tag{14}$$

where, $a_1 = \frac{k_{hnf}}{k_f}\frac{1}{Pr}$.

The boundary conditions are:

$$\left.\begin{aligned} &p(0) = 1 + \lambda q(0), s(0) = -\frac{k_f}{k_{hnf}}Bi\left\{1 - \theta(0)\right\}, f(0) = 0, \phi(0) = 1\, at\, \eta = 0 \\ &\theta(\infty) = 0, p(\infty) = 0, \phi(\infty) = 0 \end{aligned}\right\} \tag{15}$$

Step 2: Initial guesses for unknown conditions:

Since some boundary conditions are specified at infinity (η_∞) (or a sufficiently large finite value), unknown initial slopes are assumed at the wall (at η = 0). These guesses are crucial for initiating the numerical integration.

Step 3: Numerical Integration using RKF45:

The system of first-order ODEs is solved using the RKF45, which provides an adaptive step size and error control. This method ensures numerical stability and high accuracy for stiff boundary layer equations.

Step 4: Shooting and Correction Technique:

After integration, the obtained solution is checked against the specified boundary conditions at the far-field (as $\eta \to \infty$). If discrepancies are observed, the initial guesses are updated using a root-finding

algorithm such as the Newton–Raphson method. The process iterates until all boundary conditions are satisfied within a pre-defined error tolerance.

Step 5: Convergence Criteria and Grid Independence:
A uniform step size of $h = 0.001$ is used in the integration process. The solution is considered converged when the relative error in all boundary conditions falls below 10^{-5}. Grid independence is confirmed by repeating the numerical solution with smaller step sizes and verifying that the results remain unchanged beyond a certain precision level.

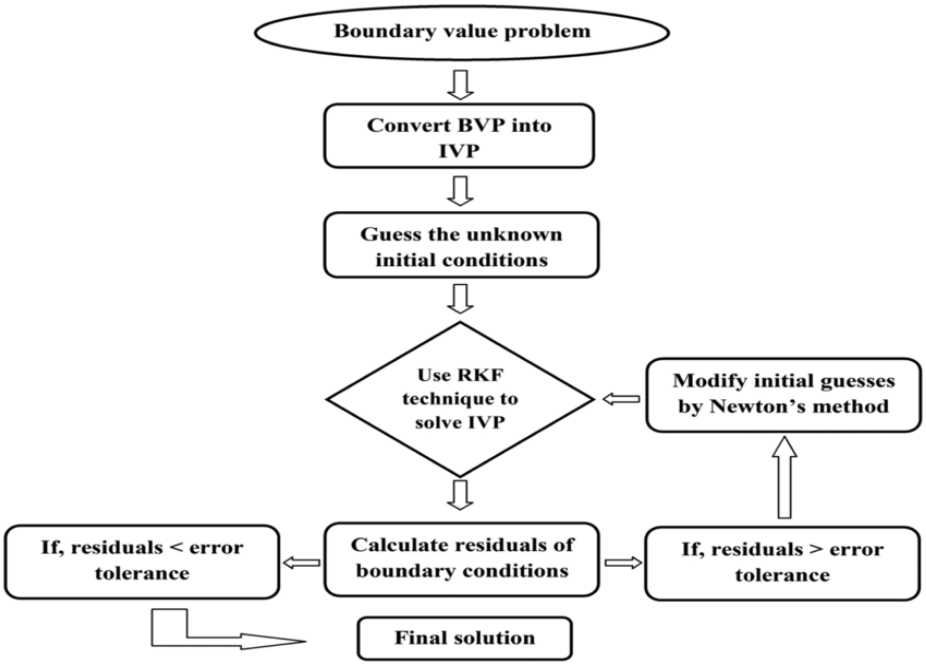

Figure 2. The flow chart of the numerical method.

5. Convergence Analysis and Grid Independence Test

5.1 Convergence Analysis

The RKF45 is known for its high accuracy, adaptive step size control and ideal for solving nonlinear ODEs. Its intrinsic formulation guarantees unconditional stability in non-linear systems experienced in nanofluid flow and MHD.

The iterations continued until the convergence criterion satisfied:

$$\boldsymbol{max}\,|u_j^{(k+1)} - u_j^{(k)}| < 10^{-5}.$$

5.2 Grid Independence Test

A grid independence test was conducted to guarantee the reliability and accuracy of the Runge Kutta–Fehlberg method. The numerical results for skin friction coefficient, Nusselt number and Sherwood number were evaluated for several grid sizes. **Table 4** demonstrates the Grid Independence analysis. showning that results become practically unchanged for $\Delta\eta \leq 0.002$. Based on this observation, a very

fine step size of $\Delta\eta$ = 0.001 was selected for all computations to ensure high resolution and numerical stability.

Table 4. Grid-independence analysis.

Step size $\Delta\eta$	Number of grid points $\left(\mathcal{N} = {}^{\eta_\infty}/_{\Delta\eta}\right)$	Sherwood-number	Skin-friction coefficient	Nusselt number
0.001	1000	0.3805	0.9585	0.5686
0.002	500	0.3805	0.9585	0.5686
0.005	200	0.3802	0.9584	0.5682
0.010	100	0.3791	0.9576	0.5672

Step size of $\Delta\eta$ = 0.001 is used throughout the analysis for optimal accuracy and the comparison validates that the results are independent of further grid refinement beyond $\Delta\eta$ = 0.002.

6. Results & Discussion

The non-linear ODEs equations in Equations (7)-(9) together with boundary conditions in Equation (10) are solved using Keller box technique to find results. In this discussion, an equal grid size $\Delta\eta$ = 0.001 is used and solutions are obtained with an error tolerance of 10^{-5} with the parameter values Pr = 6.2, $Ec = 0.1, \phi_1 = \phi_2 = 0.02, \lambda = 0.1, M = 0.3$ $Gr = Gc = 2, K_r = 0.1, Sc = 0.6, Q = 0.1$, $Kp = 0.3, Bi = 0.1$. To have a comprehension of the physical nature of the problem, the essential elements of flow, heat and mass transfer characteristics are analysed. Numerical simulations are carried out for the governing parameters. The accuracy of numerical code is achieved by comparing the numerical outcomes of the current investigation with the earlier results of Devi and Devi (2016) and Ahmad et al. (2021) as seen in **Table 5**. It is clear from the table that a very good agreement is observed.

Table 5. Result Comparison of $-\theta'(0)$ for different values of *Pr where Ec*=0.1, *n*=1, *Kp*=2, *M*=0.3, *Gr* =*Gc*=0, *Sc*=1, K_r=0.2.

Pr	Ahmad et al. (2021)	Devi and Devi (2016)	Present result
2	0.91045	0.91135	0.911238
7	1.89083	1.89540	1.895026
20	3.35271	3.35390	3.352775
70	6.47814	6.45614	6.458249

- ***Effect on velocity field:***

Figure 3 demonstrates the consequences of the volume-fraction of *Cu* and Al_2O_3 nanoparticles on the velocity of a hybrid nanofluid. Augmenting ϕ_1 (*Cu* nanoparticles) lessens the nanofluid's velocity because of the greater flow resistance brought on by the higher density, intensified viscosity, and improved thermal dissipation. But opposite effect is observed for Al_2O_3 nanoparticles as the fluid experiences less inertia, lower viscosity, and less resistance, allowing it to flow more freely. **Figure 4** depicts the implications of *M* and *Kp* on the velocity-profile of hybrid-nanofluid. The figure clearly demonstrates that that as porosity escalates, the effective flow area decreases, leading to greater resistance, causing a consequent drop in fluid velocity. Also, the hike in *M*, introduces a Lorentz-force that counteracts the flow, diminishing the hybrid-nanofluid's velocity. **Figure 5** explains the repercussions of *Gr* and *Gc* on velocity profile. Temperature at the stretching sheet differs from that of the surrounding fluid as the thermal Grashof number escalates. Because of the buoyancy forces produced by this temperature differential, the fluid is forced upward or outward from the surface. Essentially, the stronger the buoyancy

effect, the greater the upward or outward push on the fluid, leading to an enhanced velocity. Similar scene has been witnessed in case of *Gc*. Greater concentration differences deliver stronger buoyancy effects, which lower fluid motion resistance and raise the fluid's-velocity. **Figure 6** demonstrates the consequences of thermal-slip on profile of velocity. It is clearly seen that velocity gradually diminishes when slip parameter hikes but from $\eta = 0.47$ (nearly), reverse effect has been noticed.

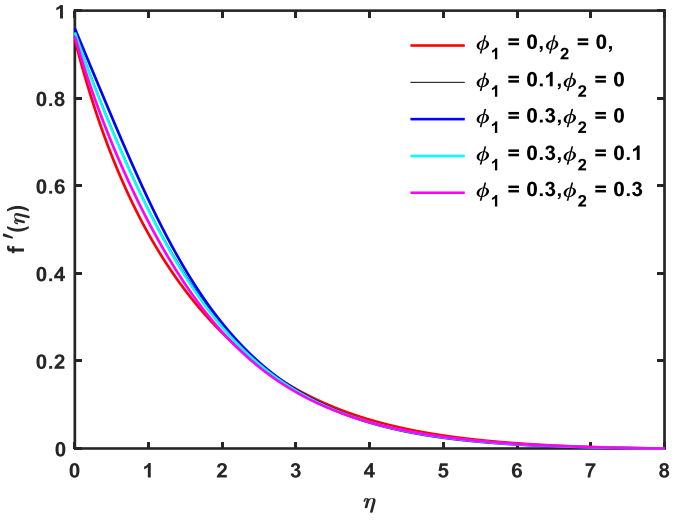

Figure 3. Illustrations of velocity with ϕ_1 and ϕ_2.

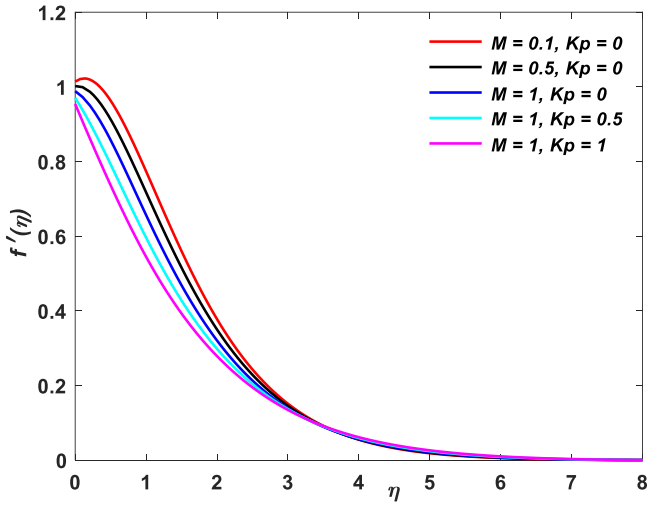

Figure 4. Illustrations of velocity with *M* and *Kp*.

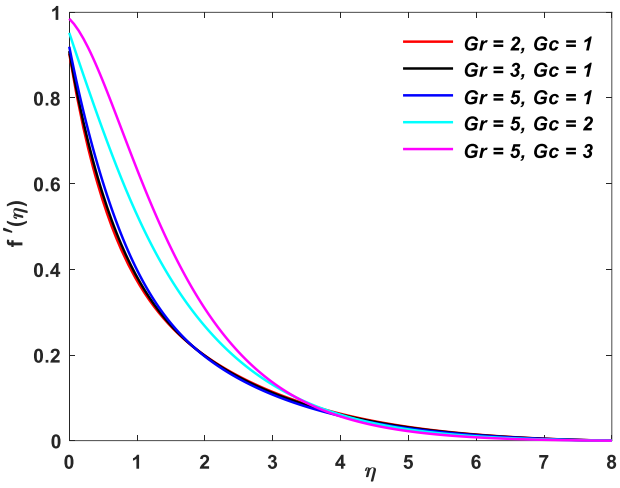

Figure 5. Illustration of velocity with *Gr* and *Gc*.

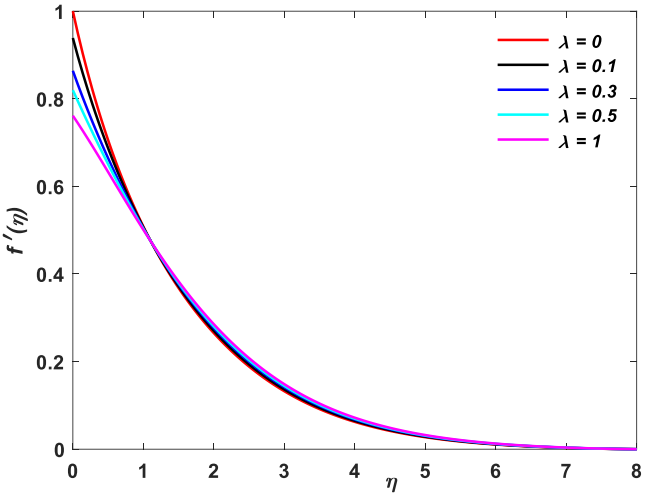

Figure 6. Illustration of velocity with λ .

- ***Effect on Temperature Field*:**

From **Figure 7**, it is concluded that, a greater volume proportion of both nanoparticles indicates more surface area is available to absorb and transfer heat. These particles are spread over the base fluid and transmit heat more efficiently from the stretching sheet to the rest of the fluid, raising the overall temperature. Also from **Figure 8**, it is determined that enhancing *M* usually raises the hybrid-nanofluid's temperature. This is because as soon as an external magnetic field is introduced to a hybrid-nanofluid, Lorentz forces are produced. These forces impede the fluid's velocity, causing energy to dissipate as heat which raises the fluid's temperature. However, the opposite effect has been observed in case of *Kp,* because increased porosity facilitates fluid flow through the porous material, generally leading to improved convection. This enhanced convection raises heat transmission away from the fluid, which lowers its temperature. **Figure 9** demonstrates the repercussions of slip parameter and Biot-number on

temperature profile. Surface convective heat transfer efficiency is enhanced with increasing *Bi*, allowing more heat to be transmitted from sheet to the hybrid-nanofluid, causes a greater fluid temperature whereas larger thermal slip parameter implies a weaker heat transfer between the fluid and solid-surface, meaning less heat is conducted into the fluid, resulting in a drop in temperature. **Figure 10** indicates the variation of temperature with varying *Gr* and *Gc*. Enhancing both *Gr* and *Gc* leads to stronger buoyancy-driven convection due to temperature and concentration differences respectively which in turn enhances heat transfer and raises the overall temperature. It is observed from **Figure 11** that as *Ec* rises, viscous forces inside the fluid are powerful enough to transfer a large portion of its kinetic energy into heat, resulting in a rise in temperature. Also, hike in Q (> 0 heat source) means, more heat is being generated internally within the hybrid-nanofluid. This additional heat directly elevates the thermal energy of the fluid, resulting in an increased temperature whereas for $Q < 0$ acts as the heat sink produces the opposite effect.

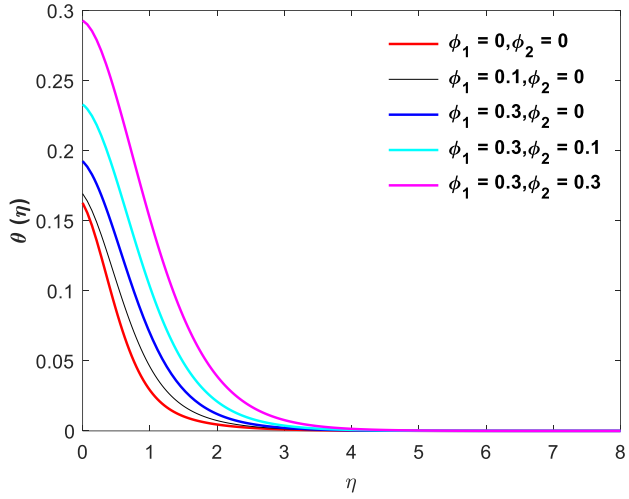

Figure 7. Illustrations of temperature with ϕ_1 and ϕ_2.

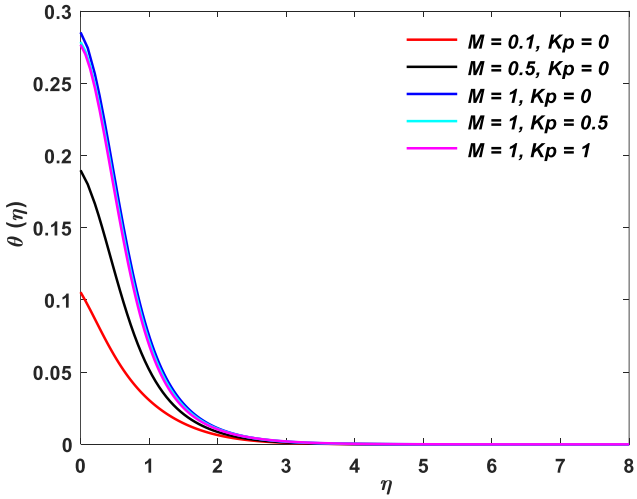

Figure 8. Impacts of *M* and *Kp* on temperature.

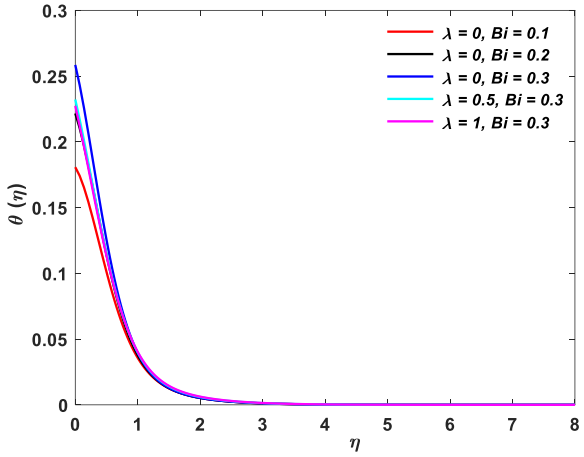

Figure 9. Illustrations of temperature with λ and Bi .

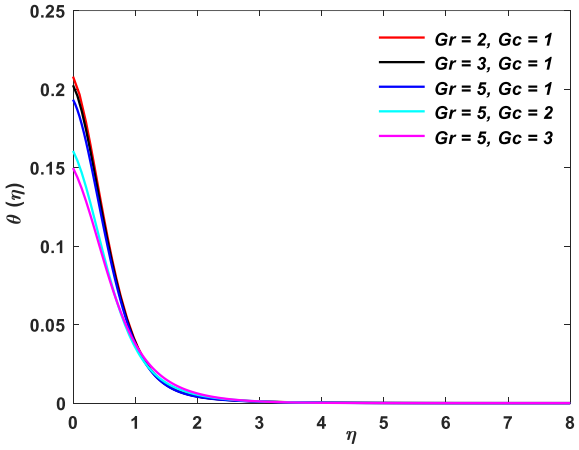

Figure 10. Impacts of *Gc* & *Gr* on temperature.

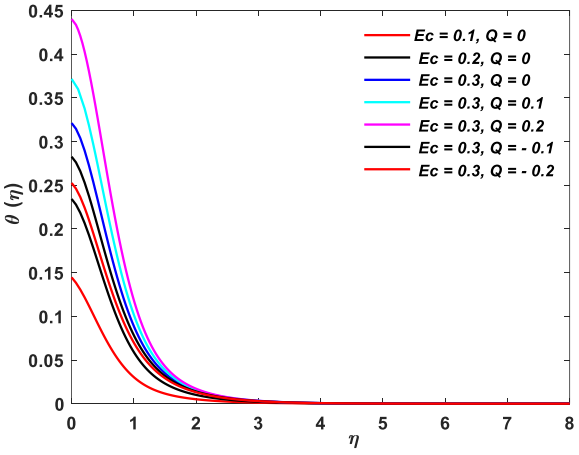

Figure 11. Impacts of *Q* and *Ec* on temperature.

- ***Effect on Concentration Field*:**

Figure 12 demonstrates the repercussions of *Sc* and K_r on concentration profile. Enhancement in Schmidt number reduces the concentration of solutes or nanoparticles in the hybrid nanofluid by slowing the diffusion process, thereby causing greater dilution and lowering mass transfer efficiency. But in case of raising K_r, when the reaction is generative, it enhances the nanoparticles particle production and retention, resulting in an overall rise in concentration. From **Figure 13**, it is observed that due to higher Grashof numbers (Both *Gr* and *Gc*), there is an elevated buoyancy, which in turn enhances convective transport and reduce diffusion, ultimately contributing to a reduction in nanoparticle concentration. **Figure 14** explains the ramifications of *M* and *Kp* on Concentration. Increasing *M* reduces convective transport, enhance diffusion, and potentially hikes the boundary layer thickness, all of which can contribute to a higher nanoparticles-concentration in the hybrid-nanofluid. Also, increased porosity may result in a thicker boundary layer, resulting in higher surface nanoparticle concentration, which ultimately hikes the concentration.

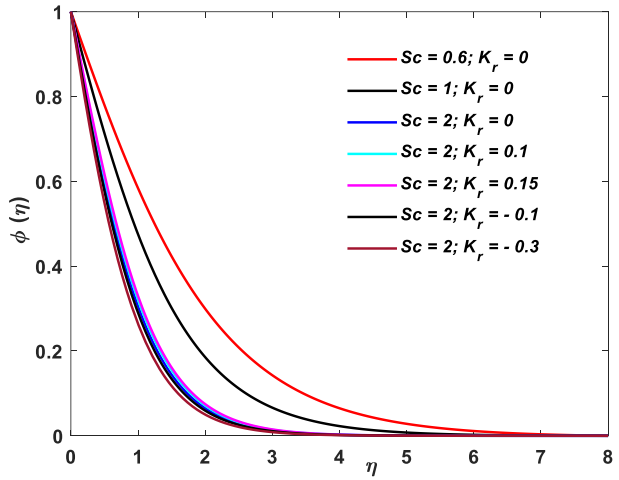

Figure 12. Impacts of *Sc* and K_r on concentration.

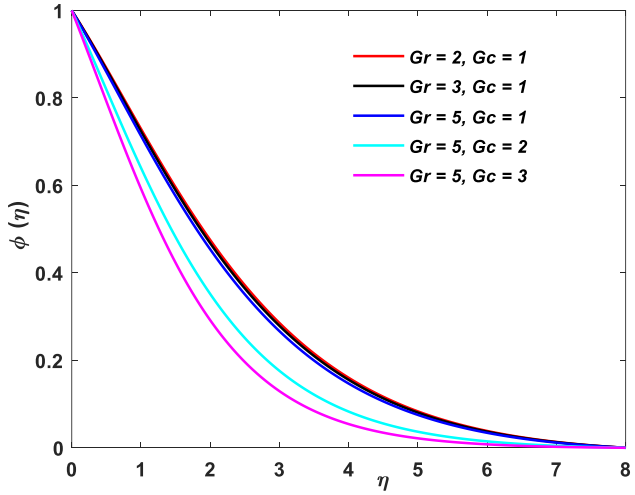

Figure 13. Impacts of *Gc* & *Gr* on concentration.

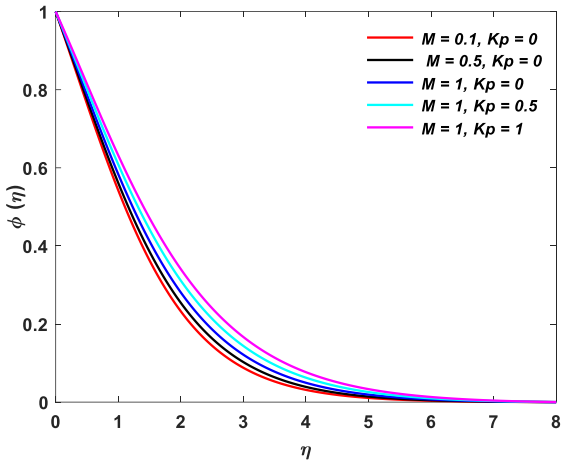

Figure 14. Repercussions of *Kp* & *M* on concentration.

- ***Effect on Entropy Generation in the Flow Analysis:***

From **Figure 15**, it is concluded that, enhancement in the M enhances the resistance to fluid motion caused by the Lorentz force, which subsequently amplifies viscous dissipation and Ohmic heating. These effects collectively result in elevated entropy generation, reflecting greater irreversibility's within the system. **Figure 16** demonstrates the consequences of A and A' on N_G. The temperature-difference parameter is commonly linked to the magnitude of thermal gradients within the system. A hike in this parameter suggests that the system permits greater heat transfer with minimal accumulation of irreversibility's, potentially reducing thermal entropy generation. Enhancement in the A' leads to greater mass transfer irreversibility's, which in turn contributes to greater entropy generation. This underscores the trade-off between concentration gradients and system efficiency, as larger concentration differences result in enhanced entropy production and diminished overall efficiency. **Figure 17** demonstrates the repercussions of B on N_G. The diffusion parameter relates to the mass diffusion rate within the fluid. As this parameter hikes, mass-transfer by diffusion becomes more prominent, resulting in greater mass transfer irreversibility's. It can be seen from **Figure 18** that rise in Br indicates stronger viscous dissipation in the system and rises entropy generation. This is because greater viscous heating leads to higher thermal irreversibility's, thus amplifying the total entropy generation.

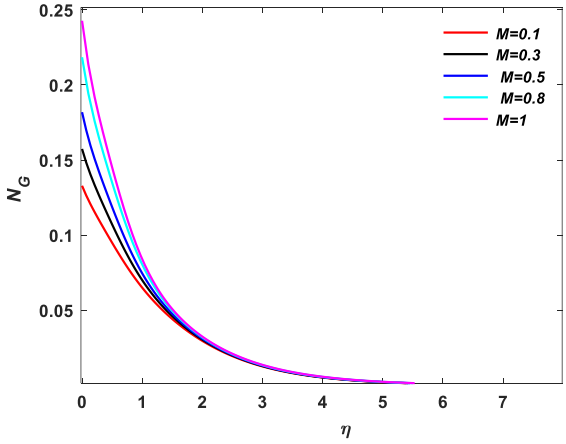

Figure 15. Repercussions of M on N_G.

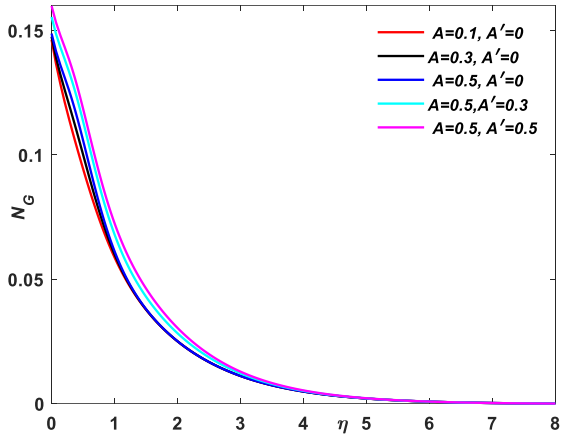

Figure 16. Repercussions of A and A' on N_G.

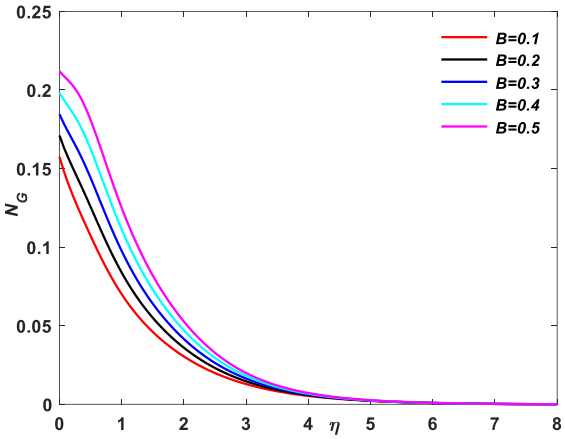

Figure 17. Repercussions of B on N_G.

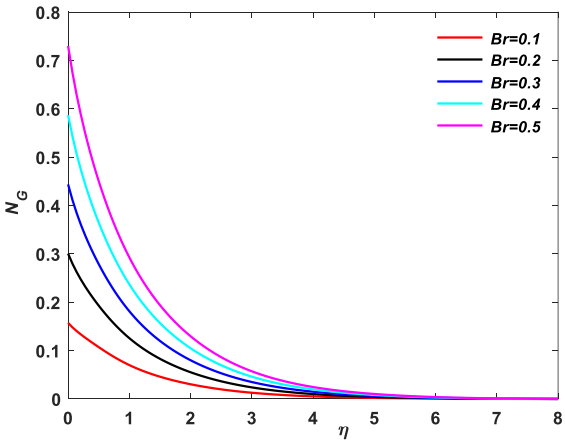

Figure 18. Repercussions of Br on N_G.

- ***Effect on Skin Friction, Nusselt Number and Sherwood Number:***

In contrast to the effect of magnetic-parameter, we can conclude from **Figure 19** and **Figure 20** that elevating ϕ_1 and ϕ_2 enhances the effective viscosity and momentum-transfer within the fluid, leading to higher surface shear stress and thus a higher skin friction coefficient. **Figure 21** makes it quite evident that augmenting the values of *Gr* reduces the impact of solutal-buoyancy, resulting in a lesser concentration driven shear at the surface and a reduction in the skin-friction coefficient against *Gc*.

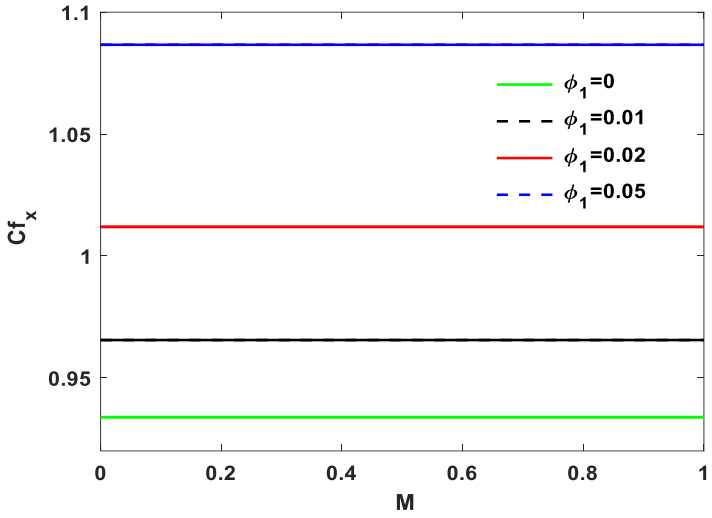

Figure 19. Skin friction coefficient for different values of ϕ_1.

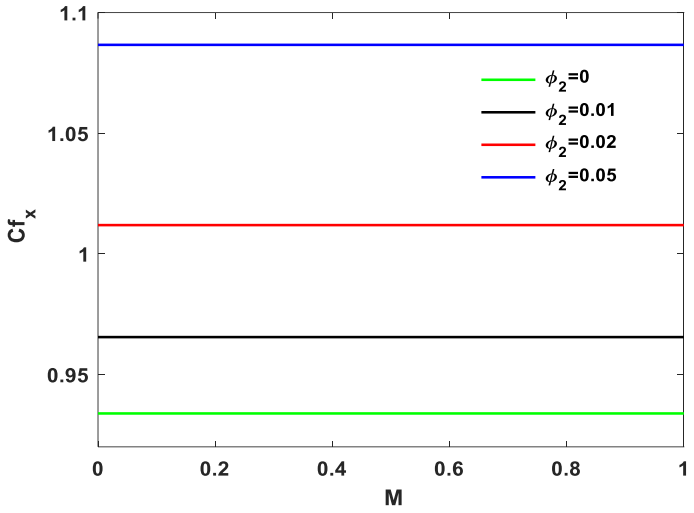

Figure 20. Skin-friction coefficient for different values of ϕ_2.

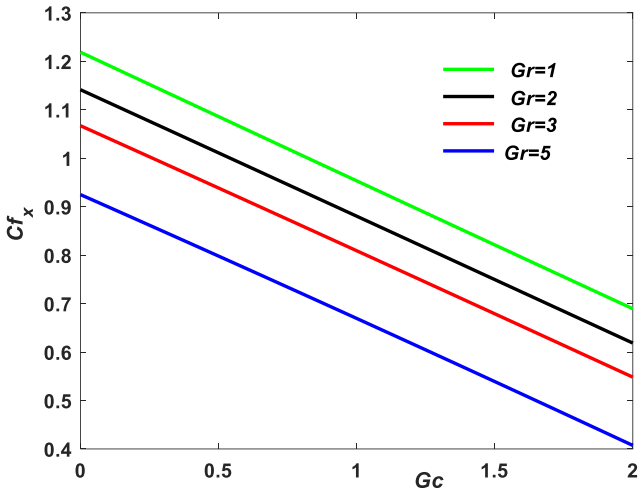

Figure 21. Skin friction coefficient for different values of Gr vs Gc.

Figure 22 demonstrates the influence of M on the Nu_x against Kp. An elevation in the M inhibits fluid flow via the Lorentz force, hence diminishing convective heat transfer irrespective of porosity. This results in decline of Nusselt-number as the augmented heat transport from flow in the porous media is reduced. From **Figure 23** it is observed that as Biot-number grows, it facilitates the fluid's heat absorption from the surface and enhancement in convective heat-transfer is seen when copper nanoparticles are added because they increase the fluid's thermal-conductivity. This synergy raises the Nusselt-number as the Bi increases against ϕ_1. **Figure 24** demonstrates the repercussions of K_r on the Sherwood-number against Sc. Augmenting the values of K_r accelerates the depletion of species near the surface, reducing the concentration gradient necessary for convective mass transfer. This leads to a decrease in Sherwood number, even when the Sc is high, as the reaction limits the effectiveness of both diffusion and convection for mass transfer.

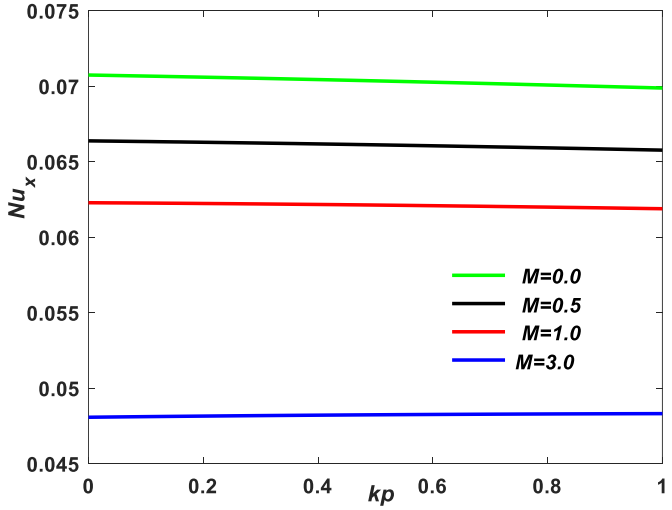

Figure 22. Nu_x for varying-values of M vs Kp.

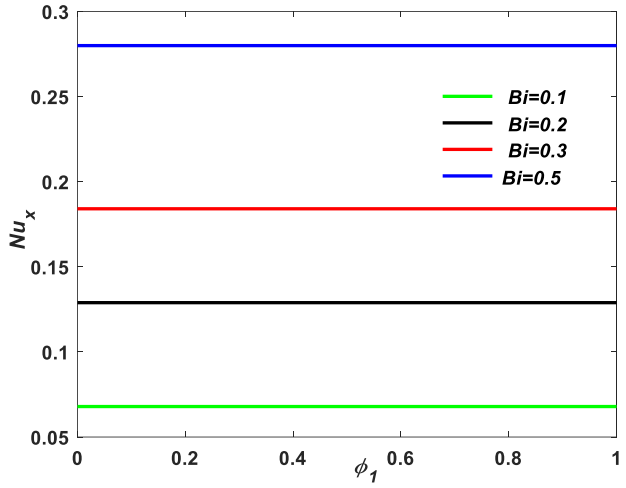

Figure 23. Nusselt-number for varying-values of *Bi* verses ϕ_1.

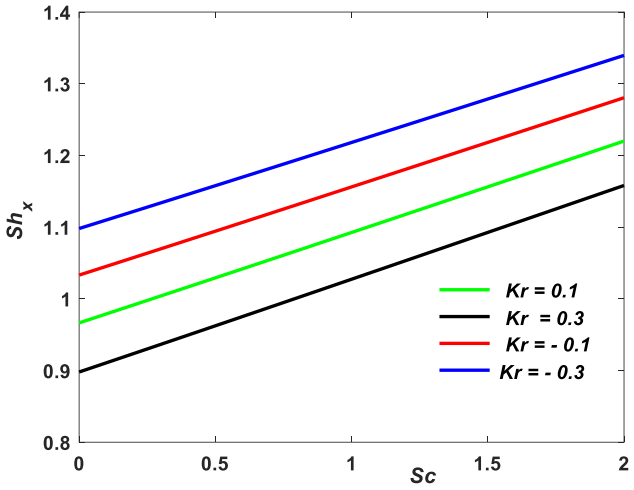

Figure 24. Sh_x for various-values of K_r versus *Sc*.

- ***Comparison with Single Nanoparticle Nanofluid*:**

The aim of this comparison is to pick out the contributions of each nanoparticle in terms of thermal and transport behavior type & evaluate their combined impact. So, a comparative study was done between two conventional fluids: *Cu / water*, Al_2O_3 / *water* and Al_2O_3-*Cu / water* HNF to assess the performance advantages of hybrid nanofluids. The comparison was carried out under identical boundary conditions and parameter settings by selectively nullifying one nanoparticle's volume fraction while keeping the total volume fraction constant.

From **Table 6**, it is evident that HNF invariably outperforms the single nanoparticle cases. Hybrid nanofluid attains 16% higher heat transfer rate than Al_2O_3/ *Water* and 11% higher than *Cu / water*. This

enhancement is due to the combined thermal behavior of aluminum oxide & copper, Since *Cu* delivers high thermal conductivity, while Al_2O_3 improves suspension stability and specific heat. These findings are consistent with the trend, since Devi and Devi (2017) also concludes that Al_2O_3–*Cu*/water HNF has upto 17% higher heat transfer compared to *Cu/water*. In terms of mass transfer (Sherwood number), the hybrid nanofluid displayed improved behavior compared to *Cu/water* and similar/slightly improved performance over Al_2O_3*/water*. In terms of skin friction, the hybrid fluid displays moderate shear stress at the wall, balancing the high momentum diffusivity of *Cu* with the relatively lower viscosity increase from Al_2O_3.

Also from **Table 6**, the entropy generation in the HNF was found to be lower than that of the conventional fluids under equivalent operating conditions, especially in regimes dominated by viscous dissipation and Joule heating.

Overall, the results reinforce the advantage of using hybrid nanofluids over single nanoparticle formulations, offering better thermal performance, balanced hydrodynamic behaviour, and improved system efficiency for a range of engineering applications.

Table 6. Comparison of single nanoparticle nanofluids and HNF for $Ec = 0.1$, $n = 2$, $Kp = 2$, $M = 1.0$, $Gr = Gc = 2$, $Sc = 1$, $K_r = 0.5$, $Bi = 0.5$.

Nanofluid type	Skin-friction coefficient	Nusselt number	Sherwood number	Entropy generation
Al_2O_3 / *water*	0.4886	1.5866	0.948	0.142
Cu / *water*	0.5379	1.6621	0.954	0.147
Al_2O_3-*Cu* / *water*	0.5144	1.8455	0.962	0.128

7. Practical Applications

The findings of this study could lead to major advancements for real-world industrial and engineering processes. The present study enables the outcomes directly applicable to the microchannel cooling systems, optimization and design of heat exchangers, and thermal regulation in electronic devices. In addition, the capacity to control entropy generation and flow stability could have a significant impact for renewable energy technologies, such as bio-photoreactors, solar collectors, and geothermal reservoirs where mass and heat transfer is essential. These insights offer a pathway for developing thermal management systems and next-generation energy-efficient cooling.

8. Conclusion

Considering combined effects of buoyancy, Newtonian heating, viscous dissipation, this study analyses the boundary layer hybrid-nanofluid (*Cu*-Al_2O_3 / *water*) flow, as it passes a linear stretching sheet.
Below are the conclusions:

- Enhancing *Gr, Gc* and *M* raises temperature as well as concentration while reducing velocity. This is useful in electronic cooling, where controlled heat transfer and reduced flow velocity ensure efficient thermal management using magnetic and buoyancy effects.
- Reduction in the temperature and velocity of hybrid-nanofluid has been seen with the rise in *Kp*, whereas reverse-effect has been observed for concentration, highlighting its role in packed-bed reactors and porous media thermal devices.
- *Bi*, ϕ_1 and ϕ_2 elevates the Nusselt-number, enhancing heat transfer but skin-friction coefficient lowers for ϕ_1 and ϕ_2.
- There is a hike in temperature of HNF with the raise in *Ec* and *Bi*, displaying the role of viscous dissipation and surface heating to extrusion of polymers and lubrication processes.

- Chemical reaction parameter enhances the concentration whereas Schimdt number lowers the concentration of HNF.
- Brinkman number, Magnetic and concentration-difference parameter elevates the entropy generation whereas reduced by temperature-difference parameter, demonstrating trade-offs in energy-efficient thermal system design.
- Hike in Q (>0) elevates temperature, whereas Q (<0 heat sink), cools the system effectively. This is useful in thermal energy systems, where heat sources enhance temperature for efficient operation, while heat sinks are used to prevent overheating and maintain system stability.
- In contrast to the impact of M, elevating ϕ_1 and ϕ_2 enhances skin-friction coefficient. Opposite effect has been seen for Nusselt-number when M is elevated against Kp.
- Sherwood number elevated with the hike in K_r against Sc by limiting mass diffusion near the surface.
- Hybrid nanofluid exhibits superior heat transfer performance, with up to 16% higher Nusselt number compared to single nanofluids, proving excellent heat transfer efficiency and thermodynamic performance.
- The rate of entropy-generation was lowest in the hybrid case, indicating better thermodynamic efficiency.
- Optimal parameter combinations are necessary to minimize entropy generation and maximize thermodynamic performance.

Future Perspectives: Several extensions are still up for future research. This study may extend the model by integrating non-Newtonian fluids, unsteady flow models, examining ternary hybrid nanofluids alongside experimental validation to reinforce applicability in industrial systems. Moreover, incorporating machine learning and optimization methods may open up new possibilities for biomedical applications, for designing smart cooling system. Further, this study can be extended for a non-linear stretching sheet.

Limitations

- Single-phase Tiwari–Das approach is used in the model, assuming uniform nanoparticle distribution and neglects slip between particles and fluid.
- The analysis is confined to 2D steady laminar boundary-layer flow over a stretching sheet, which might be different from turbulent conditions and complex geometries in real-life systems.
- Non-Newtonian rheology, Radiation effects are also not incorporated in this study.
- The nanoparticles are considered to be spherical and of uniform size.

Conflict of Interest
The authors declare that they have no conflicts of interest to the content of this manuscript.

Acknowledgments
This research did not receive any funding from any source. The authors wish to thank the reviewers, Editor-in-Chief and section editors for their valuable suggestions that has contributed to improve quality of this work.

AI Disclosure
During the preparation of this work the author(s) used generative AI in order to improve the language of the article. After using this tool/service, the author(s) reviewed and edited the content as needed and take(s) full responsibility for the content of the publication.

References

Abbas, A., Hussanan, A., Ullah, Z., El-Zahar, E.R., & Seddek, L.F. (2024). Heat and mass transfer in magnetohydrodynamic boundary layer flow of second-grade nanofluid past inclined stretching permeable surface implanted in a porous medium. *International Journal of Modeling and Simulation*, 1-15. https://doi.org/10.1080/02286203.2024.2330993.

Abdelhafez, M.A., Abdalla, A.N., Abbas, I., & Elhadidi, N. (2024). Hybrid nano liquid flow with electromagnetohydrodynamic and bioconvective across a stretching sheet in a porous media with thermal buoyancy effect. *Sohag Journal of Sciences*, *9*(3), 217-225. https://doi.org/10.21608/sjsci.2024.245808.1139.

Abdou, M.M.M., & Al-Wtheeh, R.M.M. (2025). Buoyancy-driven heat and mass transfer in magnetized nanofluid with dissipative porous media. *Applied Mathematics & Information Sciences, 19*(1), 1-14. https://doi.org/10.18576/amis/190101.

Abrar, M.N. (2025). Entropy analysis of double diffusion in a darcy medium with tangent hyperbolic fluid and slip factors over a stretching sheet: role of viscous dissipation. *Numerical Heat Transfer, Part A: Applications*, *86*(10), 3337-3350.

Acharya, N., Maity, S., & Kundu, P.K. (2022). Entropy generation optimization of unsteady radiative hybrid nanofluid flow over a slippery spinning disk. *Proceedings of the Institution of Mechanical Engineers, Part C: Journal of Mechanical Engineering Science*, *236*(11), 6007-6024. https://doi.org/10.1177/09544062221115357.

Ahmad, S., Ali, K., Rizwan, M., & Ashraf, M. (2021). Heat and mass transfer attributes of copper–aluminum oxide hybrid nanoparticles flow through a porous medium. *Case Studies in Thermal Engineering*, *25*, 100932. https://doi.org/10.1016/j.csite.2021.100932.

Aly, E.H., Mahabaleshwar, U.S., Anusha, T., & Pop, I. (2023). Exact solutions for MHD and radiative wall jet hybrid nanofluid flow over a permeable surface with velocity slip and convective boundary conditions. *ZAMM-Journal of Applied Mathematics and Mechanics/Zeitschrift für Angewandte Mathematik und Mechanik*, *103*(1), e202100261. https://doi.org/10.1002/zamm.202100261.

Arif, M., Raju, S.K., Vajravelu, K., Kumam, P., Raju, C.S.K., & Raju, S.V.S.R. (2023). Physical intuition of entropy generation in a mixed convective hybrid nanofluid flow with chemical reaction, cross-diffusion, and transpiration. *Heat Transfer*, *51*(8), 7250-7286. https://doi.org/10.1002/htj.22643.

Aziz, A., Jamshed, W., Ali, Y., & Shams, M. (2020). Heat transfer and entropy analysis of Maxwell hybrid nanofluid including effects of inclined magnetic field, Joule heating and thermal radiation. *Discrete & Continuous Dynamical Systems-Series S*, *13*(10), 2667-2685. https://doi.org/10.3934/dcdss.2020142.

Devi, S.A., & Devi, S.S.U. (2016). Numerical investigation of hydromagnetic hybrid Cu–Al2O3/water nanofluid flow over a permeable stretching sheet with suction. *International Journal of Nonlinear Sciences and Numerical Simulation*, *17*(5), 249-257. https://doi.org/10.1515/ijnsns-2016-0037.

Devi, S.U., & Devi, S.A. (2017). Heat transfer enhancement of Al_2O_3-Cu/water hybrid nanofluid flow over a stretching sheet. *Journal of the Nigerian Mathematical Society*, *36*(2), 419-433.

El-Dawy H.A., El-Amin, M. (2021) Effects of viscous dissipation and Joule heating on micropolar hybrid nanofluid in a stretching/shrinking channel including thermal/solar radiation. https://doi.org/10.21203/rs.3.rs-710400/v1.

Farooq, U., Jan, A., Hilali, S.O., Alhagyan, M., & Gargouri, A. (2024). Bioconvection study of MHD hybrid nanofluid flow along a linear stretching sheet with buoyancy effects: local non-similarity method. *International Journal of Heat and Fluid Flow, 107*, 109350. https://doi.org/10.1016/j.ijheatfluidflow.2024.109350.

Hayat, A.U., Khan, H., Ullah, I., Ahmad, H., Alam, M.M., & Bilal, M. (2024). Numerical exploration of the entropy generation in tri-hybrid nanofluid flow across a curved stretching surface subject to exponential heat source/sink. *Journal of Thermal Analysis and Calorimetry, 149*(19), 10017-10029. https://doi.org/10.1007/s10973-024-13774-3.

Ibrahim, W., & Shankar, B. (2013). MHD boundary layer flow and heat transfer of a nanofluid past a permeable stretching sheet with velocity, thermal and solutal slip boundary conditions. *Computers & Fluids, 75*, 1-10. https://doi.org/10.1016/j.compfluid.2013.01.014.

Joyce, M.I., Kandasamy, J., & Sivanandam, S. (2023). Entropy generation of Al_2O_3–Cu/water flow with convective boundary conditions through a porous stretching sheet with slip effect, Joule heating and chemical reaction. *Mathematics, 28*(1), 18. https://doi.org/10.3390/mca28010018.

Kandukoori, R.C., Janapatla, P., & Chakraborty, A. (2025). Magneto hydrodynamics hybrid nanofluid flow across an exponentially stretching sheet in the presence of variable viscosity and thermal slip: entropy generation. ZAMM-*Journal of Applied Mathematics and Mechanics/Zeitschrift für Angewandte Mathematik und Mechanik*, 105(6), e70107.

Keblinski, P., Phillpot, S.R., Choi, S.U.S., & Eastman, J.A. (2002). Mechanisms of heat flow in suspensions of nano-sized particles (nanofluids). *International Journal of Heat and Mass Transfer, 45*(4), 855-863. https://doi.org/10.1016/S0017-9310(01)00175-2.

Khalatbari, S., Jalili, P., Jalili, B., & Ganji, D.D. (2025). Investigating the improvement of heat transfer and flow characteristics of hybrid nanofluids: a comprehensive review. *Proceedings of the Institution of Mechanical Engineers, Part E: Journal of Process Mechanical Engineering*. https://doi.org/10.1177/09544089251318785.

Khan, N., Abbas, N., Shaheen, A., & Shatanawi, W. (2025). Models based analysis of radiative induced MHD hybrid nanofluid flow over an exponentially stretching sheet. *International Journal of Modern Physics B*, *39*(03), 2550033.

Khan, U., Zaib, A., Bakar, S.A., Roy, N.C., & Ishak, A. (2021). Buoyancy effect on the stagnation point flow of a hybrid nanofluid toward a vertical plate in a saturated porous medium. *Case Studies in Thermal Engineering, 27*, 101342. https://doi.org/10.1016/j.csite.2021.101342.

Khan, W.A., & Pop, I. (2010). Boundary-layer flow of a nanofluid past a stretching sheet. *International Journal of Heat and Mass Transfer*, *53*, 2477-2483.

Krishna, M.V., Ahammad, N.A., & Chamkha, A.J. (2021). Radiative MHD flow of Casson hybrid nanofluid over an infinite exponentially accelerated vertical porous surface. *Case Studies in Thermal Engineering, 27*, 101229. https://doi.org/10.1016/j.csite.2021.101229.

Mahapatra, T.R., & Gupta, A.S. (2002). Heat transfer in stagnation-point flow towards a stretching sheet. *Heat and Mass Transfer*, *38*(6), 517-521. https://doi.org/10.1007/s002310100215.

Mahmood, Z., Rafique, K., Abd-Elmonem, A., Suoliman, N.A., Kumar, A., & Mukalazi, H. (2025). Analyzing thermal performance and entropy generation in time-dependent buoyancy flow of water-based hybrid nanofluid over a rotating sphere with ternary nanoparticle shape factor. *Journal of Computational Design and Engineering, 12*(1), 80-99. https://doi.org/10.1093/jcde/qwae067.

Naqvi, S.M.R.S., Manzoor, U., Waqas, H., Liu, D., Naeem, H., Eldin, S.M., & Muhammad, T. (2024). Numerical investigation of thermal radiation with entropy generation effects in hybrid nanofluid flow over a shrinking/stretching sheet. *Nanotechnology Reviews, 13*(1), 20230171. https://doi.org/10.1515/ntrev-2023-0171.

Ogunseye, H.A., Tijani, Y.O., & Sibanda, P.P. (2020). Entropy generation in an unsteady Eyring–Powell hybrid nanofluid flow over a permeable surface: a lie group analysis. *Heat Transfer, 49*(6), 3374-3390. https://doi.org/10.1002/htj.21778.

Oztop, H.F., & Abu-Nada, E. (2008). Numerical study of natural convection in partially heated rectangular enclosures filled with nanofluids. *International Journal of Heat and Fluid Flow*, *29*(6), 1326-1336. https://doi.org/10.1016/j.ijheatfluidflow.2008.04.009.

Rafique, K., Mahmood, Z., Adnan, Khan, U., Farooq, U., & Emam, W. (2025). Computational analysis of MHD hybrid nanofluid over an inclined cylinder: variable thermal conductivity and viscosity with buoyancy and radiation effects. *Modern Physics Letters B, 39*(17), 2550033. https://doi.org/10.1142/S0217984925500332.

Rana, S., Madkhali, H.A., Nawaz, M., & Alharbi, S.O. (2023). Numerical study of Cattaneo-Christov heat transfer in MHD Carreau-Yasuda hybrid nanofluid subjected to buoyancy force. *ZAMM-Journal of Applied Mathematics and Mechanics/Zeitschrift Für Angewandte Mathematik Und Mechanik*, *103*(12), e202300037. https://doi.org/10.1002/zamm.202300037.

Sakkaravarthi, K., & Reddy, P,B.A. (2024). Entropy generation on MHD flow of Williamson hybrid nanofluid over a permeable curved stretching/shrinking sheet with various radiations. *Numerical Heat Transfer, Part B: Fundamentals*, *85*(3), 231-257. https://doi.org/10.1080/10407790.2023.2231633.

Santosh, C., & Parida, S.K. (2023). Heat transfer analysis of MHD viscous nanofluid flow over a nonlinearly stretching sheet with heat source/sink: a numerical study. *Numerical Heat Transfer, Part A: Applications*, *86*(3), 462-481. https://doi.org/10.1080/10407782.2023.2266568.

Siddappa, B., & Abel, S. (1985). Non-Newtonian flow past a stretching plate. *Zeitschrift für Angewandte Mathematik und Physik*, *36*(6), 890-892.

Sobale, S., Tawade, J.V., Bagane, P., Govindan, V., Abdullaeva, B., Ameen, H.F.M., & Batool, N. (2025). Analysis of MHD radiative flow of ternary hybrid nanofluid over a porous stretching surface. *Partial Differential Equations in Applied Mathematics*, 101267. https://doi.org/10.1016/j.padiff.2025.101267.

Suresh, S., Venkitaraj, K.P., Selvakumar, P., & Chandrasekar, M. (2012). Effect of Al_2O_3–Cu/water hybrid nanofluid in heat transfer. *Experimental Thermal and Fluid Science*, *38*, 54-60. https://doi.org/10.1016/j.expthermflusci.2011.11.007.

Tanuja, T.N., Kavitha, L., Varma, S.V.K., Raju, V.C.C., Ganteda, C.K., Obulesu, M., & Hussain, S.M. (2024). Heat and mass transfer analysis of Casson-based hybrid nanofluid flow in the presence of an aligned magnetic field: an application toward mechanical engineering. *Proceedings of the Institution of Mechanical Engineers, Part N: Journal of Nanomaterials, Nanoengineering and Nanosystems*. Advance online publication. https://doi.org/10.1177/23977914241248546.

Turkyilmazoglu, M. (2024a). Evidence of stretching/moving sheet-triggered nonlinear similarity flows: atomization and electrospinning with/without air resistance. *International Journal of Numerical Methods for Heat & Fluid Flow*, *34*(9), 3598-3614.

Turkyilmazoglu, M. (2024b). Two models on the unsteady heat and fluid flow induced by stretching or shrinking sheets and novel time-dependent solutions. *ASME Journal of Heat and Mass Transfer*, *146*(10), 101802. https://doi.org/10.1115/1.4065674.

Turkyilmazoglu, M., & Alotaibi, A. (2025). On the viscous flow through a porous-walled pipe: asymptotic MHD effects. *Microfluidics and Nanofluidics*, *29*(6), 33. https://doi.org/10.1007/s10404-025-02808-5.

Uygun, N., & Turkyilmazoglu, M. (2025). MHD non-Newtonian Bingham fluid flow and heat transfer over a rotating disk regulated by a uniform radial electric field. *International Journal of Heat and Fluid Flow*, *116*, 109899.

Vajravelu, K., & Rollins, D. (1992). Heat transfer in an electrically conducting fluid over a stretching surface. *International Journal of Non-Linear Mechanics*, *27*(2), 265-277. https://doi.org/10.1016/0020-7462(92)90085-L.

Varatharaj, K., Tamizharasi, R., & Vajravelu, K. (2025). Ternary hybrid nanofluid flow and heat transfer at a permeable stretching sheet with slip boundary conditions. *The European Physical Journal Special Topics*, *234*(8), 2293-2316.

Varatharaj, K., Tamizharasi, R., Sivaraj, R., & Vajravelu, K. (2024). Simulation of MHD-Casson hybrid nanofluid dynamics over a permeable stretching sheet: effects of heat transfer and thermal radiation. *Journal of Thermal Analysis and Calorimetry*, *149*(15), 8693-8711.

Waini, I., Ishak, A., & Pop, I. (2021). Hybrid nanofluid flow towards a stagnation point on an exponentially stretching/shrinking vertical sheet with buoyancy effects. *International Journal of Numerical Methods for Heat & Fluid Flow, 31*(1), 216-235. https://doi.org/10.1108/HFF-04-2020-0215.

Wang, X.Q., & Mujumdar, A.S. (2007). Heat transfer characteristics of nanofluids: a review. *International Journal of Thermal Sciences*, *46*(1), 1-19. https://doi.org/10.1016/j.ijthermalsci.2006.06.010.